Near-Atomic Resolution Structure of J-aggregated Helical Light Harvesting Nanotubes

Arundhati P. Deshmukh,[†1] Weili Zheng,[†2] Chern Chuang,[3] Austin D. Bailey,[1] Jillian A. Williams,[1] Ellen M. Sletten,[1] Edward H. Egelman,*[2] Justin R. Caram*[1]

[†]Co-first authors; *Corresponding authors egelman@virginia.edu (EHE), jcaram@chem.ucla.edu (JRC)

[1]*Department of Chemistry and Biochemistry, University of California, Los Angeles, 607 Charles E. Young Dr. East, Los Angeles, CA-90095, United States.* [2]*Department of Biochemistry and Molecular Genetics, University of Virginia, Charlottesville, VA-22908, United States.* [3]*Chemical Physics Theory Group, Department of Chemistry, University of Toronto, 80 St. George Street, Toronto, Ontario M5S 3H6, Canada.*

Function-oriented design of supramolecular self-assemblies represents a foundational goal in chemistry. Especially, chromophore self-assemblies display extreme photophysical changes from their monomers that are sensitive to the nanoscale molecular arrangements. Slip-stacked arrangements in J-aggregates lead to red shifts (>200 nm) and enhanced quantum yields. Actively introducing specific molecular arrangements using supramolecular chemistry provides a platform to tune the excitonic couplings and avail exotic photophysical properties. However, the nanoscale molecular arrangements have not yet been directly observed in these solution-state assemblies. Here, we present a high-resolution structure of the prototypical biomimetic light harvesting nanotubes (LHNs) of an amphiphilic cyanine dye (C8S3-Cl). We achieve a 3.3 Å resolution with helical reconstruction of cryo-EM images, directly visualizing the atomic scale parameters and

packing arrangements that control the excitonic properties. Our structure clearly shows a brick layer arrangement of the molecules as opposed to the previously thought herringbone arrangement. Furthermore, we identify a new non-biological supramolecular motif – interlocking sulfonates, that may be responsible for the slip-stacked packing and ultimately the J-aggregate nature of LHNs. This motif may be relevant towards other amphiphilic self-assemblies, in general and provides a new chemical handle on predictable self-assemblies.

Introduction

Structure-property relationships form the crux of modern materials design where specific functional properties can be induced using synthetic and structural tools. Among biological and organic materials, robust supramolecular interactions provide a reliable and tunable handle for controlling functional properties. This is the most apparent in chromophore supramolecular aggregates, whose photophysical properties are significantly altered upon self-assembly. π-conjugated chromophores form supramolecular polymeric architectures (nanotubes, sheets or bundles) that display highly modulated photophysical properties (altered absorption/emission wavelengths, optical linewidths, quantum yields) relative to the respective monomers. [1–3] These drastic changes in absorption and emission (by 2000-3000 cm^{-1}) arise due to long-range excitonic coupling – transition dipole moments of individual molecules coherently interact over long distances and form delocalized Frenkel excitons. This is in stark contrast to solid-state semiconductors where the electronic/optical properties are governed by the valence and conduction bands derived from nearest-neighbor coupling between building blocks.[3] The delocalization of excitons in supramolecular chromophore assemblies can be leveraged to achieve emergent behaviors such as wide spectral tunability (spanning the visible through shortwave infrared wavelengths), efficient ultrafast excitonic energy transport, high photochemical stability,

and excitonic superradiance, which provide a compelling basis for modern optoelectronic and energy harvesting technologies.[4–6]

Natural photosynthetic antennae employ similar excitonic coupling to efficiently channel the incoherent solar energy to a reaction center for charge separation.[2] Fenna, Mathews and Olson solved the structure of the light harvesting complex from green sulfur bacteria--the first X-ray structure of a pigment antenna protein--uncovering the three-dimensional chromophore arrangement that enables excitonic energy transfer from the chlorosome to the reaction center.[7] This led to spectroscopic studies that revealed the complex nature of the excitonic coupling and the ultrafast energy transfer pathways within the (now named) Fenna-Mathews-Olson (FMO) complex as well as other natural photosynthetic antennae.[8–12] Inspired by such naturally evolved photosynthetic antennas, many scientists have sought to engineer synthetic supramolecular analogs, which leverage exciton delocalization and energetic disorder to drive energy transport at the nanoscale.[13–19]

The classic signatures of excitonic coupling are shifts and narrowing in optical absorption of chromophores upon concentration or in poor solvents. Jelley and Scheibe concurrently observed this phenomenon in 1936, where absorption of a pseudoisocyanine dye red-shifted and narrowed upon concentration, a phenomenon later named ‘J-aggregation’.[20,21] Frenkel, Kasha, Davydov, and Kuhn progressively developed a theoretical description of this behavior invoking how transition dipole moment coupling among close-packed chromophores creates extended excitonic states, which interact collectively with electromagnetic fields.[22–24] Transition dipole moment couplings, and thereby, the observed excitonic shifts are sensitive to the geometric arrangements due to the directional nature of Coulombic interactions. Kasha’s foundational work relates the observed spectral shifts to the underlying molecular arrangements in one-dimensional systems. According

to this model, H-aggregates with co-facial packings of molecules have blue-shifted optical spectra, whereas J-aggregates with head-to-tail arrangements have red-shifted spectra.[23] Recent work has shown several extensions of this theory, illustrating that excitonic coupling and thereby, the spectral shifts and the degree of narrowing are sensitive the geometric arrangements of the molecules, nature of various intermolecular interactions, structural and/or energetic disorder, as well as the overall aggregate topology (linear, 2D sheets, tubes *etc*.).[25–27] However, achieving fine-control over all these parameters requires a high-resolution structure of the underlying supramolecular self-assemblies.

Though the excitonic coupling in the chromophore aggregates is strong, the self-assembly itself is driven by weak dispersive forces such as π–π stacking, van der Waals interactions, and entropically driven micellization, leading to structural disorder and the absence of supramolecular phonon modes despite the long-range periodicity.[28–30] Like other amphiphiles, molecular aggregates often cannot be crystallized due to the absence of symmetry elements that can be packed into a three-dimensional space group. For instance, the only helical filaments that may be packed into a crystal so that all subunits are in an equivalent environment contain either 2, 3, 4 or 6 subunits per turn.[31,32] Even if they do crystallize, the solid-state crystal structures will not be representative of the inherent solution state assembly that causes the emergent excitonic phenomena. As a result, such chromophore aggregates have not been amenable to traditional crystallographic approaches rendering any high-resolution structural information highly elusive. The structures are also known to be extremely sensitive to mild changes in their environments, limiting the scope of solution state techniques (e.g. nuclear magnetic resonance).[33,34] Cryo-EM has recently emerged as the dominant technique in structural biology for determining the atomic structure of proteins and viral assemblies.[31] The widely used plunge freezing method of sample

preparation ensures the preservation of the native solvated structure. Despite the recent cryo-EM surge among biological self-assemblies, only a few examples of high-resolution structures exist in soft matter and none among supramolecular chromophore aggregates.[31]

Here, we present a high-resolution cryo-EM structure of a model supramolecular aggregate – light harvesting nanotubes (LHNs) of amphiphilic cyanine dye C8S3. We start with the optical spectroscopy of the LHNs, followed by the high-resolution cryo-EM density maps and the atomic-level structure of the inner wall. We discuss important structural features clarified in the high-resolution structure, their relevance towards the excitonic properties and chemical design. We demonstrate the consistency between the cryo-EM structure and the Frenkel exciton model by reproducing the experimental spectra. Finally, we discuss the impact of small chemical modifications on the excitonic spectra and their implications towards motifs of self-assembly.

Results and Discussions

Light Harvesting Nanotubes (LHNs)

Originally synthesized in 1995 by Dähne and co-workers, amphiphilic cyanine dye 3,3'-bis(3-sulfopropyl)-5,5',6,6'-tetrachloro-1,1'-dioctylbenzimidacarbocyanine or C8S3-Cl (Figure 1a, inset), aggregates into double-walled nanotubes and bundled morphologies.[35] The presence of long hydrophobic alkyl chains and the hydrophilic sulfonate groups rationalized the bilayer micelle-like self-assembly into the double-walled nanotubes. Also known as light harvesting nanotubes (LHNs), the double-walled nanotubes of C8S3-Cl (shown in Figure 1b), have been explored extensively as a model excitonic system that mimics the structural complexity of natural photosynthetic antenna, showing a high degree of exciton superradiance, ultrafast energy transport and micron scale exciton migration at room temperature.[5,13,36,37] As shown in Figure 1a, the

aggregated LHNs have a red-shifted absorption from the monomer, a signature of J-aggregation. The absorption line shape of the LHNs displays characteristic features with two sharp low energy peaks and several shoulder peaks at higher energies (Figure 1a). Previous studies have assigned the sharp peaks at 589 and 599 nm to polarization of excitons along the tube axis of outer and inner walls respectively, called as outer wall parallel ($OW_{\parallel}$) and inner wall parallel ($IW_{\parallel}$) peaks, respectively.[38,39] Polarization perpendicular to the tube axis results in several broader shoulder peaks at higher energy, labelled as $OW_{\perp}$ and $IW_{\perp}$ peaks in Figure 1a.[38] Selective reduction of outer wall chromophores allows one to isolate of the inner wall spectra from the double-walled nanotube.[39] Figure 1c shows the absorption and linear dichroism (LD) spectra of the isolated inner wall LHNs with four distinct peaks (two parallel and two perpendicular). The presence of four distinct peaks in the inner wall spectra previously led researchers to propose the herringbone model with two molecules per unit cell.[39] LHNs also possess a strong circular dichroism signature, though the structural origin of this chirality is yet to be elucidated.[38,40–43]

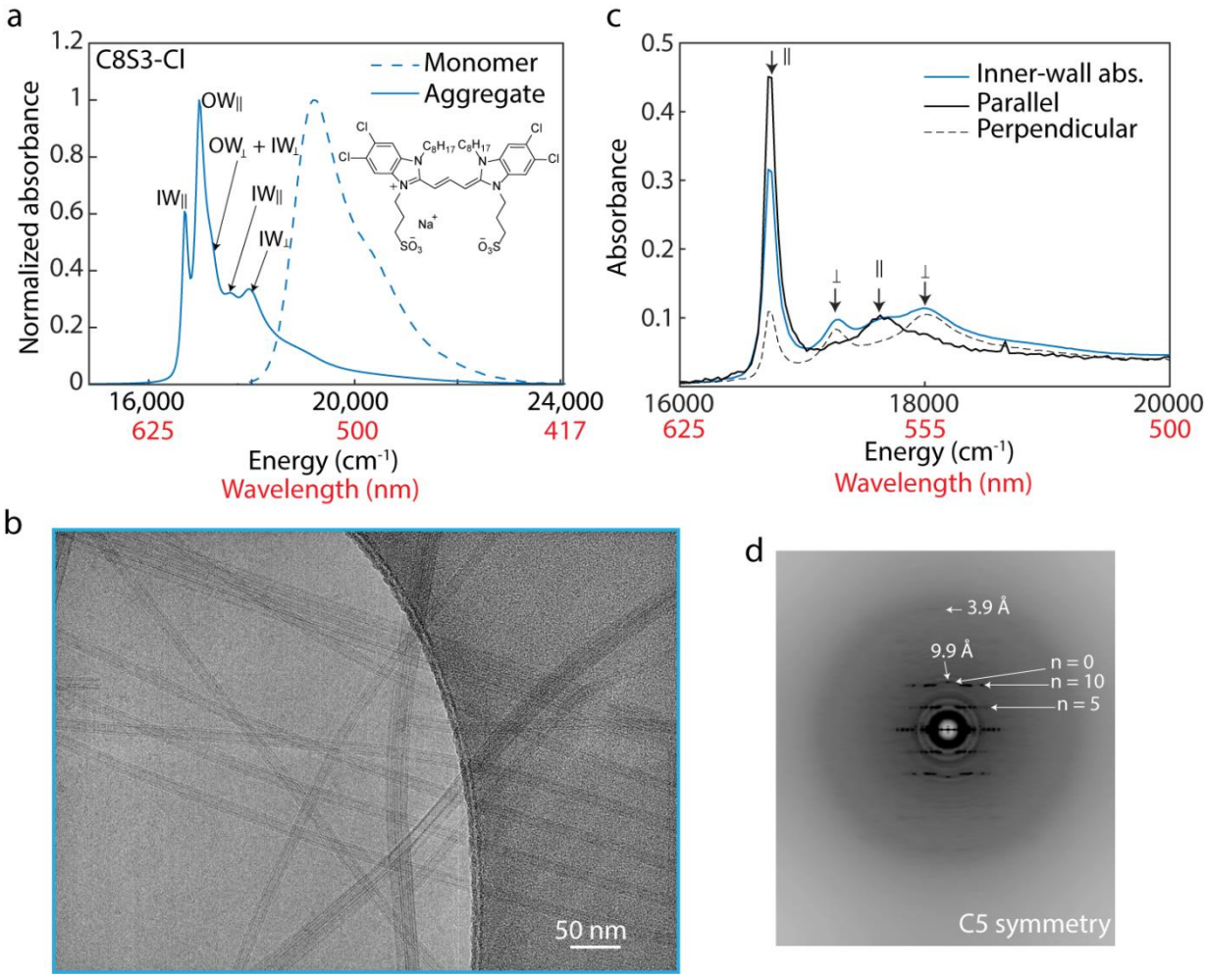

Figure 1. Light harvesting nanotubes (LHN) of amphiphilic cyanine dye C8S3-Cl, a. absorption spectra of C8S3-Cl monomer in methanol (dashed line) and J-aggregated LHNs in 30 % v/v methanol:water mixture (solid line), (*inset*) structure of C8S3-Cl, b. representative cryo-EM micrograph of LHNs showing double-walled nanotubular morphology, c. linear dichroism spectra of isolated inner wall LHNs with four peaks, and d. averaged power spectrum of the LHNs.

Extended Data Table 1 shows a literature survey of structural studies on pristine LHNs, their methodologies and key findings. As shown in Extended Data Table 1, all the nanoscale structural information was derived from low-resolution electron microscopy, excitonic modeling, and molecular dynamics simulations that were validated by comparing to the optical spectra. But the complex nature of excitonic couplings which may include additional van der Waals or charge transfer interactions make such spectral assignments ambiguous.[44,45] All the nanoscale molecular packing parameters were either obtained from simulated models or extrapolated from molecular

crystals. Solution-based structural techniques such as small angle X-ray scattering are not stand-alone and require additional modeling for data interpretation.[46] Native-state experimental probes such as cryo-electron tomography (cryo-ET) uncovered several mesoscale structural details such as the double-walled nature of LHNs, twisted and straight bundle structures, though the resolution was not high enough to resolve the nanoscale molecular packings.[13]

High-resolution structure of the LHNs

Figure 1d shows a power spectrum of the LHNs averaged from the power spectra of tens of thousands of segments of length 414.7 Å. The meridional layer line (corresponding to n = 0 Bessel function) is at 1/(9.9 Å), showing a helical rise of 9.9 Å per asymmetric unit. A striking feature in the power spectrum is the presence of weak layer lines extending out as far as 1/(3.9 Å), providing evidence for local order in the self-assembled nanotubes. The observation of layer lines corresponding to Bessel functions of order n = 0, 5, 10 etc. further suggests a possible C5 rotational symmetry in addition to the helical symmetry. We use these parameters as a starting point to iteratively reconstruct the tube density for both outer and inner walls, shown in Figure 2.

We obtain a cryo-EM map for the inner wall at 3.3 Å resolution, and the outer wall 4.3 Å with a helical rise of $h = 9.9$ Å and twist of $\gamma = 33.6°$ for both the walls. The inner wall has a higher resolution as it is more ordered, possibly due tighter packing and protection from the solvent environment. The diameters obtained from the reconstructed densities are ~ 63 and ~ 143 Å (Figure 2a), close to the previously reported values of 6 ± 1 nm and 13 ± 1 nm for the inner and outer walls respectively.[39] As seen in Figure 2a-b, the outer wall density shows some grooves denoted by blue arrows. Thus, the outer wall can be better described as broad helically wound strips with a gap in between each asymmetric unit, rather than uniformly packed molecular helices.

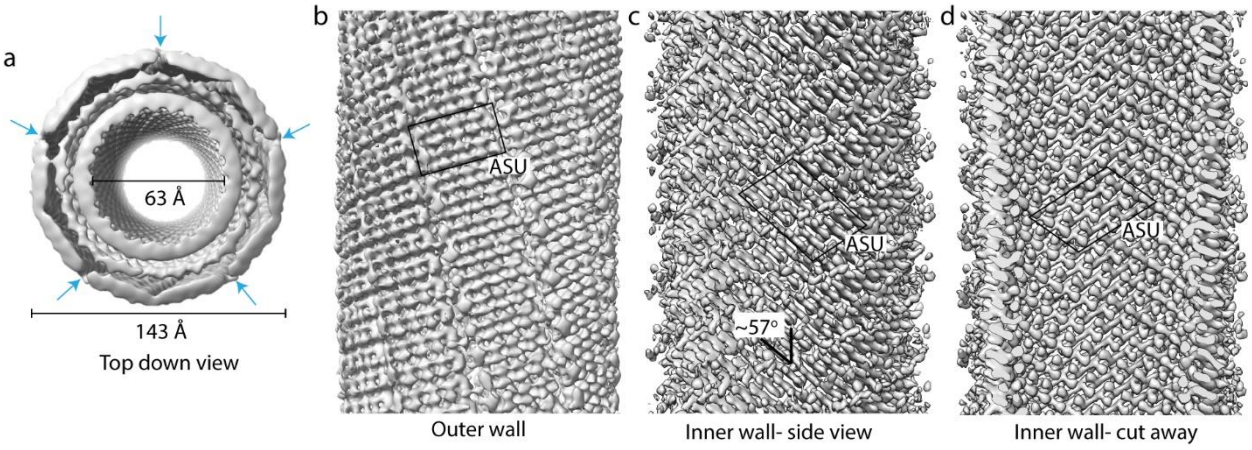

Figure 2. Cryo-EM density maps of the LHNs a. top view of the double-walled nanotubes with diameters labelled, b. side view of the outer wall, c. side view, and e. cut away view of the inner wall.

The reconstructed inner wall density was fit with a molecular model, and an overlay of the two is shown in Figure 3a-b. We observed excellent correlation between the molecular model and the reconstructed density. The asymmetric unit (ASU) for inner wall contains six molecules (Figure 3c and Extended Data Figure 1). Five ASUs go around the circumference of the tube to complete a single turn (Figure 3d), and each adjacent turn is related by the helical symmetry parameters (h, γ). Figures 3e-f show space filling models for two such segments (color coded magenta and cyan). We note an ambiguity in the assignment of the helical hand which is inherent to any helical reconstruction from 2D projections.[47,48] For protein or peptide assemblies containing α-helices, the known hand of the α-helices (right-handed for L-amino acids) allows for unambiguous determination of the hand at any resolution better than ~ 4.5 Å.[31,49] Similarly, for β-stranded structures, the hydrogen bonding pattern allows for determining the absolute hand at better than ~ 2.8 Å resolution.[49] However, C8S3-Cl being an achiral planar molecule presents no clear preference for a single handedness. We report the structure with a right-handed 5-start helix for simplicity but the LHNs may exist in an ensemble of both right- and left-handed helices.

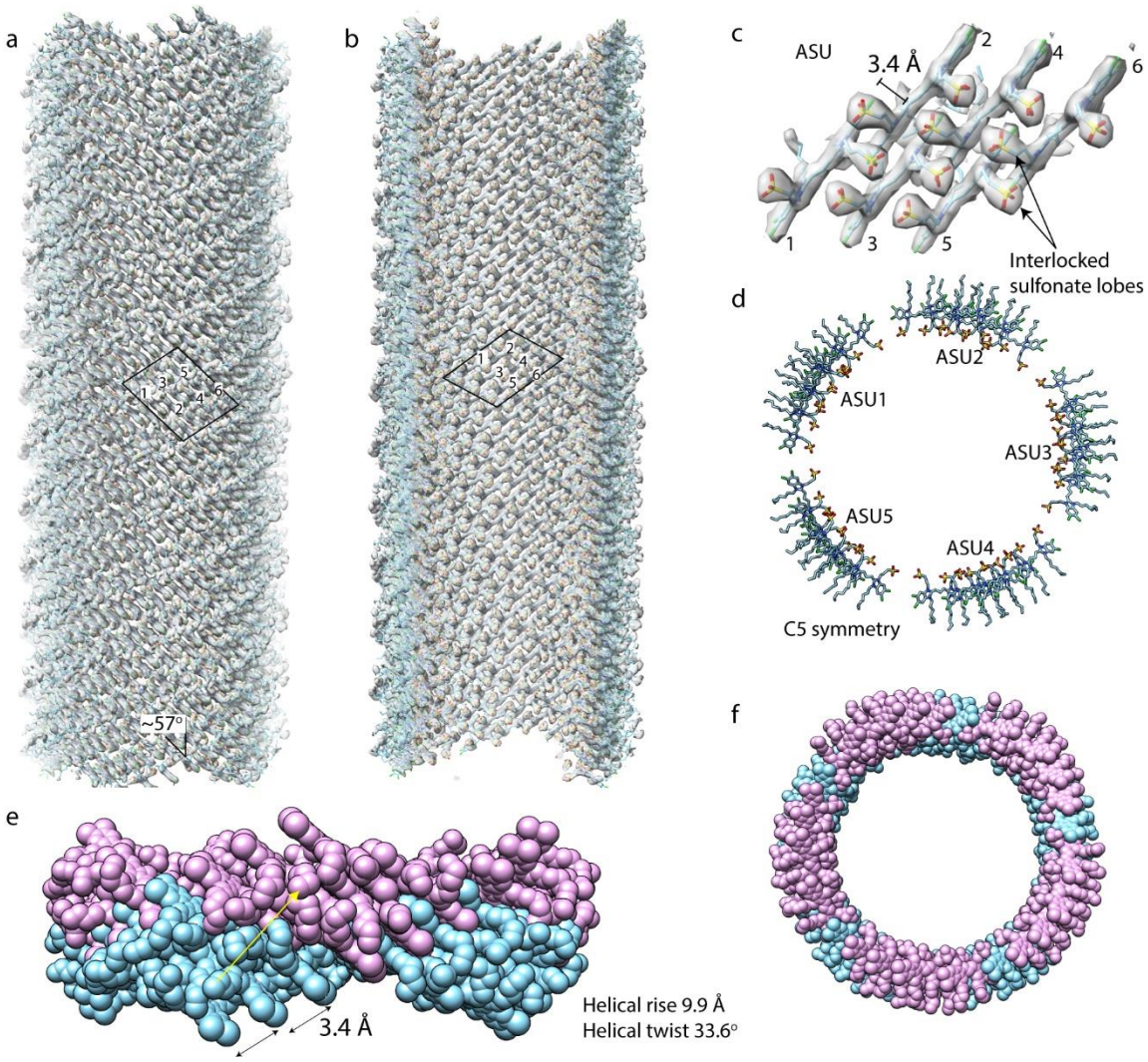

Figure 3. Molecular model for the inner wall LHNs, a-c. Inner wall density overlaid with the structure showing excellent agreement with the reconstructed density, a. side view, and b. cut away view, c. structure of asymmetric unit (ASU) with six non-identical molecules, d. top-down view of the five repeats of the ASUs around the circumference, e. side view and f. top-down view of two helically translated repeats of the ring in part d.

Insights from the high-resolution structure

Both brick layer and herringbone type arrangements had been proposed for the nanoscale structure of the LHNs with the plausibility of each geometry still open to debate.[6,39,46,50,51] However, Figure 3 clearly shows a slip stacked packing of the dye molecules with a brick layer type arrangement leading to a structural reassignment with direct ramifications towards the excitonic properties. The herringbone geometry was originally motivated by apparent symmetry-

breaking in the optical spectra of the isolated inner wall, resulting in multiple parallel and perpendicular polarized peaks (Figure 1c). While this was a reasonable assumption with the limited structural knowledge at the time, our results clearly show that this symmetry breaking, in fact, arises from six unique molecular environments in the ground state. The $\pi-\pi$ stacking distance is 3.4 Å and the slip between adjacent molecules is 9.0 Å. Our results present a direct experimental confirmation of these supramolecular packing parameters, that are often used as input parameters in the Frenkel exciton model for calculating the excitonic spectra.

Furthermore, we observe regular crisscrossed pattern of the lobes in the lumen of the inner wall (Figure 3b-c and Extended Data Figure 2). These lobes are assigned to the sulfonate groups from neighboring dye molecules, where a sulfonate from the neighboring dye stabilizes the delocalized positive charge on polymethine chromophore. Previously, the role of the sulfonate was thought to impart hydrophilicity in the amphiphile; however, our results indicate the sulfonate groups play an essential role in the self-assembly. We believe the interlocking sulfonates are responsible for the slip-stacked packing geometry that is crucial for the J-aggregate behavior (optical red shifts, high superradiance) of the LHNs. Several chemical handles (sterics, H-bonding, etc.) have been used to enforce a slip-stacked packing in other chromophores.[28,52] However, this interlocking motif was completely unknown until now and none of the previously proposed models for the LHNs include this feature (Extended Data Table 1).

Due to the lower resolution of the outer wall map, we could not obtain a high-resolution structure for the outer wall. Instead, we fit the outer wall density to a geometry optimized model with manual constraints, shown in Extended Data Figure 3. We focus on the locations of the sulfonate groups as well as conjugated dye backbone that are better resolved in the cryo-EM map (Figure 2). Some of the unique structural features of the outer wall are clearly resolved in the cryo-

EM map as well as in the fitted model. Rather than a uniform molecular packing like the inner wall, the outer wall shows helically wound strips separated by gaps between each ASU with the overall symmetry parameters preserved, C_5 rotational symmetry with the helical symmetry parameters of rise $h = 9.9$ Å and angle $\gamma = 33.6°$. Within each of the helical strips, the conjugated backbone of the molecules follows a slip-stacked brick-layer pattern similar to the inner wall albeit with eight molecules per ASU. The sulfonate groups within the densely packed bands also follow an interlocking pattern as the inner wall, while those near the gaps are more disordered and less resolved. In Figure 2a, we observe some continuous density in the middle of the two walls. While we do not know the origin of this density, it should be noted that this does not correspond to the alkyl groups since we do not observe a continuous arm extending from the dye backbone, similar to the sulfonate chains.

Dimerized Frenkel exciton model for optical spectra

Optical properties of the LHNs and other excitonic systems are computed using the Frenkel exciton Hamiltonian.[53] The couplings are based on specific molecular packing arrangements which, until now, would be estimated from simulations (Extended Data Table 1). Here, we reconstruct the excitonic structure of the inner wall and reproduce the absorption, linear and circular dichroism spectra using the structural information from the cryo-EM structure. For simplicity, we propose a minimal dimerized Frenkel exciton model. Instead of using all six molecules in the ASU which is computationally expensive, we separate them into three adjacent pairs of molecules and average over their positions by assuming a helical symmetry with $(h_d, \gamma_d) = (h/3, \gamma/3)$ while retaining the C_5 rotational symmetry (Figure 4a). This reduces the number of molecules within an ASU to two while keeping a reasonable level of atomistic details

of the original structure. A detailed description of the methodology is given in Supplementary Information (SI): Section 1.

Based on the dimer model and the associated helical-rotational symmetry, the excitonic structure of an infinitely long inner wall can be described by a collection of 2×2 matrices $H_{k,k'}(l, l')$, where $k = 0, \ldots, 4$ is the rotational quantum number, k' is the quasimomentum associated with the helical symmetry and $l, l' = 1,2$.[26,54] These matrices are obtained by block-diagonalizing the full Hamiltonian H by applying the Bloch theorem, and the matrix elements of H are calculated based on the cryo-EM structure. The corresponding excitonic couplings are calculated using the transition charges method.[55] In practice, this Hamiltonian with parameters estimated from the cryo-EM model and quantum chemistry calculations only gives two bright states. To resolve this inconsistency, we break the dimer symmetry by adding to $H_{\parallel}$ and $H_{\perp}$ an effective intra-dimer coupling matrix ΔH:

$$\Delta H = \begin{bmatrix} \frac{\Delta\varepsilon}{2} & \Delta J \\ \Delta J & -\frac{\Delta\varepsilon}{2} \end{bmatrix} \quad (1)$$

where $\Delta\varepsilon$ and ΔJ are free parameters subjecting the on-site energies ε_1 and ε_2 and the intra-dimer coupling J_{12} such that the locations and relative brightness of the absorption peaks of the experimental values. The exact origin of ΔH is unclear as a full account of the possible types of intermolecular interactions (e.g. charge-transfer, ground state dipoles etc.) requires higher-level computations. However, the high-resolution structure presented here forms a benchmark for the geometric parameters that the excitonic couplings depend so sensitively upon. Once ΔH is given, we adopt the expressions provided in Didraga et al. to calculate various linear spectra and compare to experimental measurements.[56]

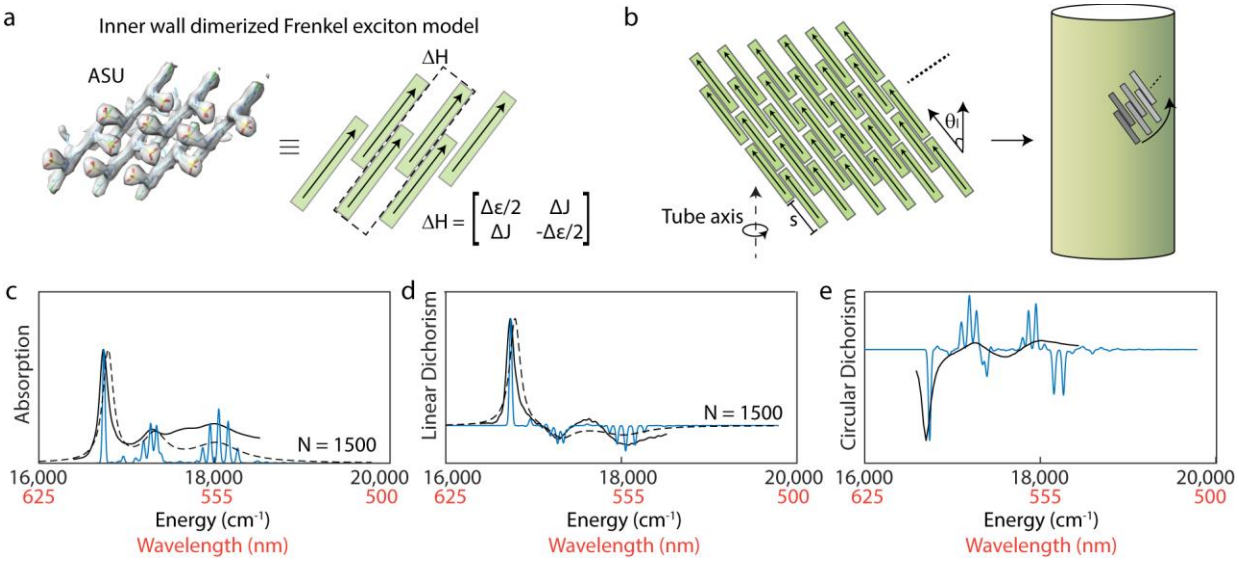

Figure 4. Dimerized Frenkel exciton model for the inner wall based on the cryo-EM structure, a. asymmetric unit (ASU) as viewed from inside the tube with intra-dimer coupling matrix ΔH, b. schematic showing the relevant geometric parameters and construction of the nanotube from the ASU, c-e. fitting the model to the experimental spectra for c. absorption, d. linear dichroism, and e. circular dichroism spectra of the isolated inner wall LHNs. Solid black lines: experimental spectra; blue lines: calculated spectra from 1500 monomer nanotube ($M = 150$); dashed black lines: calculated spectra with periodic boundary conditions and added Lorentzian broadenings.

The resulting absorption, linear dichroism, and circular spectra are shown in Figure 4c-e, showing reasonable agreement with the experiments. Extended Data Figure 4 shows the calculated spectra for aggregates of different sizes. The fitted parameters used in ΔH are $\Delta\varepsilon = 1076.1$ and $\Delta J = 171.3\ \mathrm{cm}^{-1}$. The longer the aggregate length, the more dispersed are the spectral features. From these simulations, we estimate the coherence size of the bright excitonic states in the inner wall under the experimental condition to be $1000 < N_{coh} < 1500$. While reasonable agreements have been met with the linear absorption and linear dichroism spectra, the circular dichroism spectra are less than ideal. In particular, the high frequency (positive-valued) shoulder is not reproduced with the model. We hypothesize that some degree of aggregate bundling is resulting in a slightly modulated CD spectrum.

We consider two constraints to this model set by the long and short-range excitonic couplings (details in SI Section 1). The first condition from the long-range coupling predicts the energy gap between the parallel- and the perpendicular-polarized peaks:

$$\Delta E_{\perp/\parallel} = H_{\perp}(l,l) - H_{\parallel}(l,l) = \frac{2\pi\,\mu_0^2}{r\,A_0}\sin^2\theta_l \qquad (1)$$

The second constraint relates the short-range excitonic couplings and the energy gap between the two perpendicular-polarized peaks and places an upper limit on the short-range couplings. Eq. (1) leads to $\Delta E_{\perp/\parallel} = 495\ \mathrm{cm}^{-1}$, which agrees remarkably well with the experimental value of $489\ \mathrm{cm}^{-1}$, a testament to the consistency between the cryo-EM structure and the Frenkel exciton model. We note that the dimerized model is fully consistent with it regardless of the magnitude of ΔH adopted.

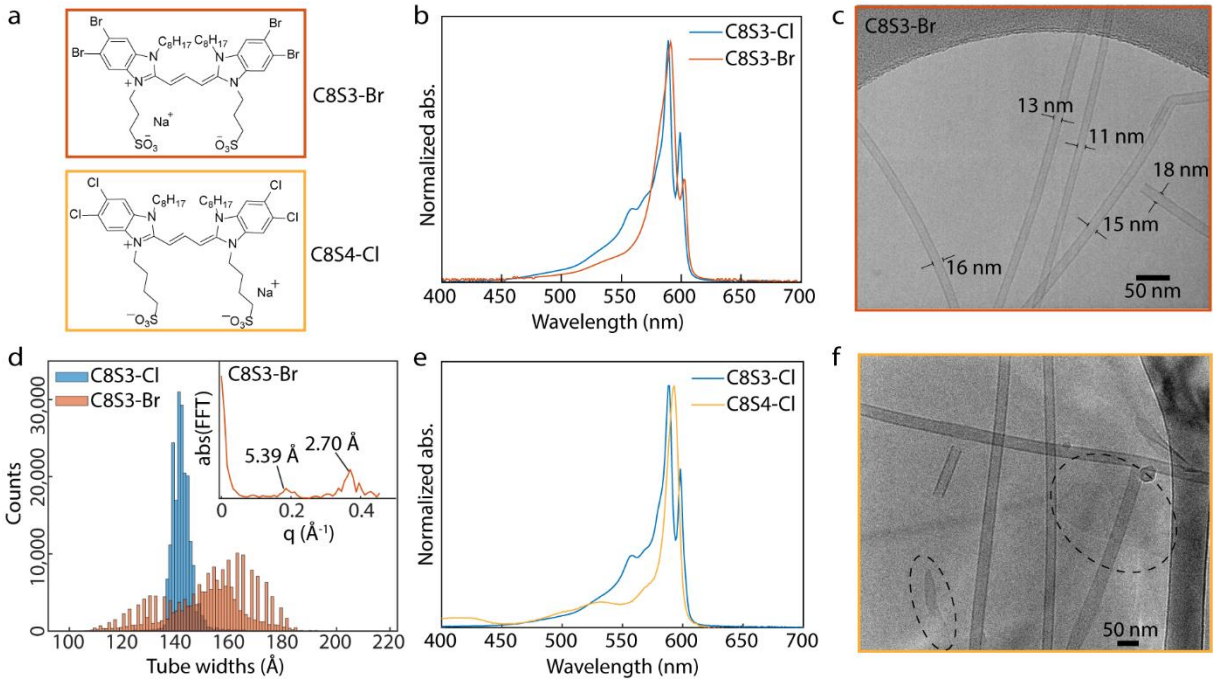

Figure 5. Impact of chemical modifications on the self-assembly, a. structures of the dyes C8S3-Br and C8S4-Cl, b. normalized absorption spectra of C8S3-Cl aggregates (pristine LHNs) and C8S3-Br aggregates, c. cryo-EM micrograph of C8S3-Br aggregates showing double-walled nanotubular morphology with variable tube diameters labelled on the image, e. histograms of C8S3-Cl and C8S3-Br tube widths over ~10^4 segments, *(inset)* Fourier transform of C8S3-Br histogram showing the step size of

the discretized tube widths, c. normalized absorption spectra of the LHNs and C8S4-Cl aggregates, and d. cryo-EM micrograph of C8S4-Cl aggregates showing nanotubes and sheets (dashed circles).

Impact of chemical modifications on the self-assembly

To explore the structural sensitivity of self-assembly, we tested two different chemical modifications to the C8S3-Cl scaffold – length of the sulfonate chains and halogen substitution (Figure 5a).[35,57] Kriete et al. found that replacing the four Chlorine atoms with the larger Bromine increases the diameter of the double-walled nanotubes while conserving the molecular packing.[57] Figure 5b shows overlayed normalized absorptions of the prototypical LHNs and C8S3-Br aggregates. Besides the slight broadening and red shift of the $IW_{||}$ and $OW_{||}$ peaks, most spectral features are well-conserved. Cryo-EM of C8S3-Br aggregates also shows a well-conserved double-walled nanotubular morphology (Figure 5c). However, C8S3-Br nanotubes had varying tube diameters unlike the uniform tube widths of the pristine LHNs. Using the larger molecule size and assuming the same packings and symmetry parameters as the pristine LHNs, one would expect the nanotubes to be only slightly wider by ~ 1%. This surprising observation led us to analyze the widths of ~10^4 nanotube segments, histogrammed in Figure 5d. C8S3-Cl shows a single narrow peak centered at ~ 140 Å, but C8S3-Br shows a much wider distribution spreading from 110 Å – 180 Å. As seen from Figure 5d, both inner and outer wall diameters of C8S3-Br nanotubes seem to increase or decrease in sync and the inter-wall separation remains the same.

Because of the variable diameters, we could not readily reconstruct the C8S3-Br nanotubes to obtain a 3D map. In principle, a massive data set might be collected to obtain a few relatively homogeneous subsets, as was previously done for a spindle-shaped viral tube.[58] Nevertheless, the C8S3-Br width histogram in Figure 5d shows an interesting feature with discrete steps rather than a continuous distribution that could be related to the nanoscale packing. A Fourier transform of

the C8S3-Br histogram is shown in the inset of Figure 5d with peaks at 2.70 Å and 5.39 Å, corresponding to the step size for the discretized widths. Based on the projection of a single chromophore adding on to the tube width (discussed in SI Section 2), we relate this step size to tube-wrapping chiral angle of $\theta = 66.4^{o}$, as opposed to the 57° angle observed in the LHNs. This signifies that the underlying molecular packing is quite distinct from the pristine LHNs.

Figure 5e shows the absorption spectra of the prototypical LHNs overlayed with the aggregates of C8S4-Cl (four methylene spacers between the conjugated backbone and the sulfonate groups instead of three in the standard LHNs). While the spectral line shape is very distinct from the pristine LHNs, cryo-EM shows a mixture of both nanotubular and sheet-like morphologies (Figure 5f). Upon careful screening of the aggregation conditions, we find that C8S4-Cl initially assembles into nanotubes that are relatively unstable and spontaneously convert into sheet-like morphology over a week as seen in Extended Data Figure 5. This instability may be explained by the fact that adding an extra carbon in the sulfonate chains can disrupt the sulfonate interlocking either by inducing more disorder or due to sterics, further hinting at the importance of this supramolecular motif in the self-assembly. Most of the other cyanine dyes in the literature with similar S4 chains have sheets as their most stable aggregate morphology.[28]

Overall, these two examples demonstrate the sensitivity of the supramolecular self-assembly to small chemical modifications. Approaching the broader goal of chemical control would require more efforts. Particularly, independent native state structural investigations are necessary as a lot of the nanoscale structural information relevant towards the stabilization of the self-assemblies can be uncovered. Going forward, the sulfonate interlocking motif can be used to guide the self-assembly of other amphiphilic systems as well.

Conclusions

We use 3D reconstruction cryo-EM images to obtain a high-resolution native-state structure of the supramolecular J-aggregated light harvesting nanotubes (LHNs). The LHNs, self-assembled from cyanine dye C8S3-Cl, continue to be a rich model system demonstrating novel excitonic behaviors such as superradiance and artificial light harvesting. Further theoretical and experimental explorations are needed to unravel all the possible couplings within this structure. Like the FMO complex, this high-resolution structure will form a solid basis for such explorations in the future. This structure also sheds light on new insights into self-assembly itself, that will inform the design of supramolecular materials.

We settle the long-standing question about the molecular arrangements (herringbone or brick layer) that are crucial towards the excitonic couplings and ultimately the unique photophysical properties of the LHNs. Our structure clearly shows the molecules in a brick layer arrangement. Symmetry breaking in the optical spectra arises from a six molecule ASU in the inner wall and eight molecule ASU in the outer wall. The ASUs follow the helical symmetry parameters of axial rise = 9.9 Å and rotation = 33.6° for both the walls. A similar observation was recently made for a synthetic peptide assembly - the lanreotide nanotubes.[49] The small peptide, previously thought to have 2 molecules in the ASU, was recently found to adapt eight slightly different conformations. These self-assembly details are only able to be observed through high-resolution native-state structure.

The sulfonate chains in both inner and outer walls show a highly conserved interlocked arrangement which enforce the slip-stacking. This slip-stacking, in turn, is responsible for the J-aggregate characteristics of the LHNs with narrow red shifted spectra and high superradiance. Not only does this provide a new chemical handle for designing excitonic materials, but this motif can also be introduced to other supramolecular self-assemblies as a configuration locking mechanism.

Small chemical modifications to the halogen atom and the sulfonate chains alter the nanotubular self-assembly in very distinct ways suggesting the need for high-resolution structures in such systems. A simple analysis of the cryo-EM images indicates distinct molecular packing for C8S3-Br even though the absorption spectrum is very similar to the LHNs. Independent native-state structural explorations provide precise supramolecular structure – excitonic property relationships, enabling predictable design of excitonic materials. Cryo-EM reconstruction, already the state-of-art in structural biology, has tremendous potential for other soft materials as well. In future, such structural explorations will complement the vast efforts in spectroscopy and modeling of excitonic supramolecular materials.

Methods

Materials

C8S3-Cl was obtained from FEW Chemicals GmbH and used without further purification. C8S3-Br was synthesized using a reported procedure.[57] C8S4-Cl was synthesized from the heterocycle 5,6-dichloro-2-methyl-1-octyl-1H-benzo[dimidazole]. We refer the readers to our earlier work for detailed synthetic procedures and characterizations of C8S3-Br as well as the precursor heterocycle.[59] Detailed synthetic procedures and characterizations for C8S4-Cl are given in Supplementary Information Section 3.

Aggregate preparation

C8S3-Cl aggregates (or LHNs) were prepared by injecting a 1.46 mM methanol solution of C8S3-Cl dye into Milli-Q water with the final conditions 0.43 mM dye and 30% MeOH (v/v) in glass vials pre-soaked in Milli-Q water for hydrophilization. The aggregate solutions were stored in parafilm sealed vials in dark at room temperature for 24 h before taking any measurements.

C8S3-Br nanotubes were prepared similarly by injecting 10 mM methanol solution of dye monomer into Milli-Q water giving 2mM, 20% MeOH as the final conditions. C8S3-Br was stored for longer time (1-2 weeks) to allow for growth of long tubes. Shorter equilibration times gave bundled aggregates for C8S3-Br. Aggregates of C8S4-Cl were formed using the same method as above, several conditions were screened for the narrow redshifted J-aggregate absorption. C8S4-Cl aggregates were prepared with final conditions of 0.2 mM dye in 10 % MeOH, unless noted otherwise.

Inner wall isolation

For isolation of inner wall spectra of C8S3-Cl LHNs, a modified form of previously reported procedure was used.[39] LHNs were prepared by dissolving C8S3-Cl monomer (2.58 mg, 2.86 μmol) into 2.4 mL spectroscopic grade methanol (Fisher). This solution was sonicated for 30 seconds to ensure complete dissolution before adding 4.76 mL Milli-Q H_2O. The solution was stored in the dark for 24 h in parafilm-sealed vials before measuring the absorbance to confirm doubled-walled LHN formation. For outer wall bleaching, 0.6 mL of 0.011 M aqueous $AgNO_3$ solution in Milli-Q H_2O was added to the LHNs vial. The vial was briefly shaken to ensure mixing, then illuminated with a flashlight until the outer wall peak was completely bleached (~ 10 min) and kept in dark subsequently. Further spectroscopic measurements were done immediately.

Spectroscopic measurements

UV-Vis and LD spectra were taken on Agilent Cary-60 spectrometer in 0.2 mm or 0.01 mm path length quartz cuvettes obtained from Starna Cells. Cuvettes were pre-soaked for several days in Milli-Q water for hydrophilization. For LD spectra, a linear polarizer (Thorlabs LPVIS050, mounted on a rotational stage) was inserted into the spectrophotometer between the sample and

lamp source. To achieve parallel or perpendicular polarizations, the polarizer was set to 0° or 90°, respectively. The instrument was blanked using the appropriate solvent for each polarizer orientation. The sample was flown at a rate of 4 mL/min through a 0.2 mm path length flow cell (Starna Cells) using a syringe pump (AL-1000, Thermo Fisher) to align the nanotubes to the direction of the flow. CD spectra were taken on ChiraScan V100 in 0.2 mm path length cuvettes while purging the chamber with N_2 gas.

Cryo-EM data collection and processing

2 μL of the LHNs or C8S3-Br double-walled nanotubes sample were applied to plasma-cleaned lacey carbon grids, followed by plunge-freezing in liquid ethane using a Leica EM GP. Data collection was carried out at liquid nitrogen temperature on a Titan Krios microscope (ThermoFisher Scientific) operated at an accelerating voltage of 300 kV. 40 movie frames were collected with defocus values range between -1 to -2.5 μm on a K3 camera (Gatan), with a total dose of ~55 electrons per $Å^2$. For C8S3-Cl double-walled nanotube, a total of 193,693 segments (384px-long) were manually boxed in EMAN2 from 2000 images, followed by testing the helical symmetry possibilities in SPIDER. The C5 rotational symmetry yielded the most reasonable map which was used as an initial map to further processing in RELION 3.0.[60] Three rounds of Refine3D, PostProcessing, contrast transfer function (CTF) refinement and Bayesian polishing were done until the map improved with recognizable small molecule features at the resolution of 3.3 Å. The helical parameters converged to a rotation of 33.6° and an axial rise of 9.9 Å per subunit. The resolution of the final reconstruction was determined by the Fourier shell correlation (FSC) between two independent half maps, which was 3.3 Å for the inner wall and 4.3 Å for the outer wall at FSC = 0.143.

For cryo-EM images of C8S4-Cl, 5 uL of the aggregate was dropped onto plasma-cleaned lacey carbon grids, and subsequently vitrified in liquid ethane using a Vitrobot Mark IV cryo-sample plunger. Images were obtained under cryogenic conditions using a Thermo Scientific Talos F200C TEM with an accelerating voltage of 200 kV.

Model building and refinement

We use the C8S3-Cl PDB model as an initial template to dock into the cryo-EM map by rigid body fitting in UCSF Chimera,[61] and then manually edited the model in Coot.[62] The refined monomeric model of C8S3 was then re-built in Chimera with helical symmetry and rotational symmetry, followed by real-space refinement with Phenix.[63] The PDB file for the atomic coordinates of the inner wall is available in the supplementary files, and the corresponding cryo-EM map for the inner and outer walls has been deposited in the EMDB with accession code EMD-27820.

References

1. Bricks, J. L., Slominskii, Y. L., Panas, I. D. & Demchenko, A. P. Fluorescent J-aggregates of cyanine dyes: basic research and applications review. *Methods Appl. Fluoresc.* **6**, 012001 (2017).

2. Brixner, T., Hildner, R., Köhler, J., Lambert, C. & Würthner, F. Exciton Transport in Molecular Aggregates - From Natural Antennas to Synthetic Chromophore Systems. *Adv. Energy Mater.* **7**, 1700236 (2017).

3. Scholes, G. D. & Rumbles, G. Excitons in nanoscale systems. *Nat. Mater.* **5**, 920–920 (2006).

4. Wang, C. & Weiss, E. A. Accelerating FRET between Near-Infrared Emitting Quantum Dots Using a Molecular J-Aggregate as an Exciton Bridge. *Nano Lett.* **17**, 5666–5671 (2017).

5. Freyria, F. S. *et al.* Near-Infrared Quantum Dot Emission Enhanced by Stabilized Self-Assembled J-Aggregate Antennas. *Nano Lett.* **17**, 7665–7674 (2017).

6. Doria, S. *et al.* Photochemical Control of Exciton Superradiance in Light-Harvesting Nanotubes. *ACS Nano* **12**, 4556–4564 (2018).

7. Fenna, R. E. & Matthews, B. W. Chlorophyll arrangement in a bacteriochlorophyll protein from Chlorobium limicola. *Nat. 1975 2585536* **258**, 573–577 (1975).

8. Maiuri, M., Ostroumov, E. E., Saer, R. G., Blankenship, R. E. & Scholes, G. D. Coherent wavepackets in the Fenna-Matthews-Olson complex are robust to excitonic-structure perturbations caused by mutagenesis. *Nat. Chem.* **10**, 177–183 (2018).

9. Panitchayangkoon, G. *et al.* Long-lived quantum coherence in photosynthetic complexes at physiological temperature. *Proc. Natl. Acad. Sci. U. S. A.* **107**, (2010).

10. Cao, J. *et al.* Quantum biology revisited. *Sci. Adv.* **6**, (2020).

11. Renger, T. Theory of excitation energy transfer: From structure to function. *Photosynth. Res.* **102**, 471–485 (2009).

12. Engel, G. S. *et al.* Evidence for wavelike energy transfer through quantum coherence in photosynthetic systems. *Nature* **446**, 782–786 (2007).

13. Eisele, D. M. *et al.* Robust excitons inhabit soft supramolecular nanotubes. *Proc. Natl. Acad. Sci.* **111**, E3367–E3375 (2014).

14. Lim, J. *et al.* Vibronic origin of long-lived coherence in an artificial molecular light harvester. *Nat. Commun.* **6**, (2015).

15. Scholes, G. D., Fleming, G. R., Olaya-Castro, A. & van Grondelle, R. Lessons from nature about solar light harvesting. *Nat. Chem.* **3**, 763–774 (2011).

16. Würthner, F., Kaiser, T. E. & Saha-Möller, C. R. J-aggregates: From serendipitous discovery to supramolecular engineering of functional dye materials. *Angewandte Chemie - International Edition* vol. 50 3376–3410 (2011).

17. Wan, Y., Stradomska, A., Knoester, J. & Huang, L. Direct Imaging of Exciton Transport in Tubular Porphyrin Aggregates by Ultrafast Microscopy. *J. Am. Chem. Soc.* **139**, 7287–7293 (2017).

18. Haedler, A. T. *et al.* Long-range energy transport in single supramolecular nanofibres at room temperature. doi:10.1038/nature14570.

19. Kreger, K., Schmidt, H. W. & Hildner, R. Tailoring the excited-state energy landscape in supramolecular nanostructures. *Electron. Struct.* **3**, 023001 (2021).

20. Jelley, E. E. Spectral absorption and fluorescence of dyes in the molecular state. *Nature* **138**, 1009–1010 (1936).

21. Scheibe, G. Über die Veränderlichkeit der Absorptionsspektren in Lösungen und die Nebenvalenzen als ihre Ursache. *Angew. Chemie* **50**, 212–219 (1937).

22. Davydov, A. S., ydov, A. S. D., Kasha, M. & Oppenheimer, M. *Theory of Molecular Excitons*. (McGraw-Hill, 1962).

23. Kasha, M. Energy Transfer Mechanisms and the Molecular Exciton Model for Molecular

Aggregates. *Radiat. Res.* **20**, 55–71 (1963).

24. Czikkely, V., Försterling, H. D. & Kuhn, H. Light absorption and structure of aggregates of dye molecules. *Chem. Phys. Lett.* **6**, 11–14 (1970).

25. Deshmukh, A. P. *et al.* Bridging the gap between H- and J-aggregates: Classification and supramolecular tunability for excitonic band structures in two-dimensional molecular aggregates. *Chem. Phys. Rev.* **3**, 021401 (2022).

26. Hestand, N. J. & Spano, F. C. Expanded Theory of H- and J-Molecular Aggregates: The Effects of Vibronic Coupling and Intermolecular Charge Transfer. *Chem. Rev.* **118**, 7069–7163 (2018).

27. Heijs, D. J., Malyshev, V. A. & Knoester, J. Decoherence of excitons in multichromophore systems: Thermal line broadening and destruction of superradiant emission. *Phys. Rev. Lett.* **95**, 177402 (2005).

28. Deshmukh, A. P. *et al.* Thermodynamic Control over Molecular Aggregate Assembly Enables Tunable Excitonic Properties across the Visible and Near-Infrared. *J. Phys. Chem. Lett.* **11**, 8026–8033 (2020).

29. Wasielewski, M. R. Self-assembly strategies for integrating light harvesting and charge separation in artificial photosynthetic systems. *Acc. Chem. Res.* **42**, 1910–1921 (2009).

30. Pandya, R. *et al.* Observation of Vibronic-Coupling-Mediated Energy Transfer in Light-Harvesting Nanotubes Stabilized in a Solid-State Matrix. *J. Phys. Chem. Lett.* **9**, 5604–5611 (2018).

31. Wang, F., Gnewou, O., Solemanifar, A., Conticello, V. P. & Egelman, E. H. Cryo-EM of

Helical Polymers. *Chem. Rev.* **122**, 14055–14065 (2021).

32. Egelman, E. H. The iterative helical real space reconstruction method: Surmounting the problems posed by real polymers. *J. Struct. Biol.* **157**, 83–94 (2007).

33. Herman, K. *et al.* Individual tubular J-aggregates stabilized and stiffened by silica encapsulation. *Colloid Polym. Sci.* **298**, 937–950 (2020).

34. Ng, K. *et al.* Frenkel excitons in heat-stressed supramolecular nanocomposites enabled by tunable cage-like scaffolding. doi:10.1038/s41557-020-00563-4.

35. Pawlik, A., Ouart, A., Kirstein, S., Abraham, H. W. & Daehne, S. Synthesis and UV/Vis spectra of J-aggregating 5,5′,6,6′-tetrachlorobenzimidacarbocyanine dyes for artificial light-harvesting systems and for asymmetrical generation of supramolecular helices. *European J. Org. Chem.* **2003**, 3065–3080 (2003).

36. Caram, J. R. *et al.* Room-Temperature Micron-Scale Exciton Migration in a Stabilized Emissive Molecular Aggregate. *Nano Lett.* **16**, 6808–6815 (2016).

37. Eisele, D. M., Knoester, J., Kirstein, S., Rabe, J. P. & Vanden Bout, D. A. Uniform exciton fluorescence from individual molecular nanotubes immobilized on solid substrates. *Nat. Nanotechnol.* **4**, 658–663 (2009).

38. Clark, K. A., Cone, C. W. & Bout, D. A. Vanden. Quantifying the Polarization of Exciton Transitions in Double-Walled Nanotubular J-Aggregates. *J. Phys. Chem. C* **117**, 26473–26481 (2013).

39. Eisele, D. M. *et al.* Utilizing redox-chemistry to elucidate the nature of exciton transitions in supramolecular dye nanotubes. *Nat. Chem.* **4**, 655–662 (2012).

40. Kirstein, S. *et al.* Chiral J-Aggregates Formed by Achiral Cyanine Dyes. *ChemPhysChem* **1**, 146–150 (2000).

41. Schade, B. *et al.* Stereochemistry-Controlled Supramolecular Architectures of New Tetrahydroxy-Functionalised Amphiphilic Carbocyanine Dyes. *Chem. – A Eur. J.* **26**, 6919–6934 (2020).

42. Roodenko, K. *et al.* Anisotropic optical properties of thin-film thiacarbocyanine dye aggregates. *J. Phys. Chem. C* **117**, 20186–20192 (2013).

43. Kriete, B., Feenstra, C. J. & Pshenichnikov, M. S. Microfluidic out-of-equilibrium control of molecular nanotubes. *Phys. Chem. Chem. Phys.* **22**, 10179–10188 (2020).

44. Bialas, D., Zhong, C., Würthner, F. & Spano, F. C. Essential states model for merocyanine dye stacks: bridging electronic and optical absorption properties. *J. Phys. Chem. C* **123**, 18654–18664 (2019).

45. Spano, F. C. Analysis of the UV/Vis and CD spectral line shapes of carotenoid assemblies: Spectral signatures of chiral H-aggregates. *J. Am. Chem. Soc.* **131**, 4267–4278 (2009).

46. Patmanidis, I. *et al.* Structural characterization of supramolecular hollow nanotubes with atomistic simulations and SAXS. *Phys. Chem. Chem. Phys.* **22**, 21083–21093 (2020).

47. Egelman, E. H. Reconstruction of Helical Filaments and Tubes. *Methods Enzymol.* **482**, 167–183 (2010).

48. Egelman, E. H. Ambiguities in helical reconstruction. *Elife* **3**, (2014).

49. Pieri, L. *et al.* Atomic structure of Lanreotide nanotubes revealed by cryo-EM. *Proc. Natl.*

Acad. Sci. U. S. A. **119**, (2022).

50. Megow, J. *et al.* Site-dependence of van der Waals interaction explains exciton spectra of double-walled tubular J-aggregates. *Phys. Chem. Chem. Phys.* **17**, 6741–7 (2015).

51. Bondarenko, A. S. *et al.* Multiscale modeling of molecular structure and optical properties of complex supramolecular aggregates. *Chem. Sci.* **11**, 11514–11524 (2020).

52. Herbst, S. *et al.* Self-assembly of multi-stranded perylene dye J-aggregates in columnar liquid-crystalline phases. *Nat. Commun.* **9**, 2646 (2018).

53. Didraga, C. *et al.* Structure, Spectroscopy, and Microscopic Model of Tubular Carbocyanine Dye Aggregates. *J. Phys. Chem. B* **108**, 14976–14985 (2004).

54. Spano, F. C., Silvestri, L., Spearman, P., Raimondo, L. & Tavazzi, S. Reclassifying exciton-phonon coupling in molecular aggregates: Evidence of strong nonadiabatic coupling in oligothiophene crystals. *J. Chem. Phys.* **127**, 184703 (2007).

55. Brent P. Krueger, Gregory D. Scholes, and & Fleming*, G. R. Calculation of Couplings and Energy-Transfer Pathways between the Pigments of LH2 by the ab Initio Transition Density Cube Method. *J. Phys. Chem. B* **102**, 5378–5386 (1998).

56. Didraga, C., Klugkist, J. A. & Knoester, J. Optical Properties of Helical Cylindrical Molecular Aggregates: The Homogeneous Limit. *J. Phys. Chem. B* **106**, 11474–11486 (2002).

57. Kriete, B. *et al.* Steering Self-Assembly of Amphiphilic Molecular Nanostructures via Halogen Exchange. *J. Phys. Chem. Lett.* **8**, 2895–2901 (2017).

58. Wang, F. *et al.* Spindle-shaped archaeal viruses evolved from rod-shaped ancestors to

package a larger genome. *Cell* **185**, 1297-1307.e11 (2022).

59. Bailey, A. D. *et al.* Tubular J-aggregates of cyanine dyes in the near-infrared. (2021) doi:10.26434/CHEMRXIV-2021-RJMVZ-V2.

60. Zivanov, J. *et al.* New tools for automated high-resolution cryo-EM structure determination in RELION-3. *Elife* **7**, (2018).

61. Goddard, T. D., Huang, C. C. & Ferrin, T. E. Visualizing density maps with UCSF Chimera. *J. Struct. Biol.* **157**, 281–287 (2007).

62. Emsley, P., Lohkamp, B., Scott, W. G. & Cowtan, K. Features and development of Coot. *Acta Crystallogr. Sect. D Biol. Crystallogr.* **66**, 486–501 (2010).

63. Adams, P. D. *et al.* PHENIX: A comprehensive Python-based system for macromolecular structure solution. *Acta Crystallogr. Sect. D Biol. Crystallogr.* **66**, 213–221 (2010).

64. von Berlepsch, H., Kirstein, S., Hania, R., Pugžlys, A. & Böttcher, C. Modification of the Nanoscale Structure of the J-Aggregate of a Sulfonate-Substituted Amphiphilic Carbocyanine Dye through Incorporation of Surface-Active Additives. *J. Phys. Chem. B* **111**, 1701–1711 (2007).

65. Lyon, J. L. *et al.* Spectroelectrochemical Investigation of Double-Walled Tubular J-Aggregates of Amphiphilic Cyanine Dyes. *J. Phys. Chem. C* **112**, 1260–1268 (2008).

66. Berlepsch, H. V, Ludwig, K., Kirstein, S. & Böttcher, C. Mixtures of achiral amphiphilic cyanine dyes form helical tubular J-aggregates. *Chem. Phys.* **385**, 27–34 (2011).

67. Krishnaswamy, S. R. *et al.* Cryogenic TEM imaging of artificial light harvesting complexes outside equilibrium. *Sci. Rep.* **12**, 1–8 (2022).

68. Patmanidis, I. *et al.* Modelling structural properties of cyanine dye nanotubes at coarse-grained level. (2022) doi:10.26434/CHEMRXIV-2022-75W3F.

Acknowledgements: This work was funded by NSF CHE 2204263 and NIH GM122510. APD thanks UCLA Graduate Division Dissertation Year Fellowship for financial support.

Competing interests: Authors declare no conflict of interest.

Corresponding authors: egelman@virginia.edu (EHE), jcaram@chem.ucla.edu (JRC)

Extended Data

Extended Data Table 1. A literature survey of structural investigations on the LHNs.

Reference	**Method**	**Key findings**
Kirstein et al., 2000[40]	Cryo-EM micrographs CD spectroscopy	Chirality in bundled nanotubes of C8O3[a]
Didraga et al. (Knoester), 2004[53]	Brick layer model informed by CD and LD Cryo-EM micrographs	Cryo-EM showed double-walled morphology of the nanotubes
Berlepsch et al., 2007[64]	Cryo-EM micrographs	Tubes formed rope-like bundles over weeks
Lyon et al. (Stevenson), 2008[65]	Cyclic voltammetry, optical spectroscopy and spectroelectrochemistry of immobilized LHNs on ITO	Initial oxidation of outer wall, followed by irreversible dehydrogenation and dimerization. Inner wall stayed relatively intact.
Eisele et a. (Rabe & Vanden Bout), 2009[37]	Atomic force microscopy and near-field scanning optical microscopy	The supramolecular structure was uniform within individual nanotubes as well as across an ensemble.
Berlepsch et al. (Bottcher), 2011[66]	Cryo-EM 3D reconstruction of mixed C8S3 and C8S2 tubes	2 nm resolution map with pitch angle of 17.3°
Eisele et al. (Knoester & Vanden Bout), 2012[39]	Redox chemistry Herringbone model fitted to absorption spectra	Excitonic decoupling of inner and outer wall Explains symmetry breaking in isolated inner wall spectra
Clark et al. (Vanden Bout), 2013[38]	Linear dichroism of double-walled nanotubes and photochemically isolated inner wall spectra	Total six transitions isolated for doubled-walled nanotubes (3 parallel and perpendicular pairs), 4 of which assigned to inner wall
Eisele et al. (Nicastro, Knoester & Bawendi), 2014[13]	Cryo-electron tomography of LHNs and bundles Herringbone model informed with absorption spectra	Hierarchical assembly of the LHNs with observations of straight and twisted bundles

Megow et al., 2015[50]	MD simulations with two molecules per unit cell in brick layer arrangement	Site dependent dispersive shifts due to van der Waals interactions explained the peak splitting
Kriete et al. (Pshenichnikov), 2017[57]	Replaced Cl atoms with Br Herringbone model fitted to absorption spectra	C8S3-Br tubes were wider than C8S3-Cl Spectral differences were attributed to higher radius of C8S3-Br tubes
Bondarenko et al. (Marrink & Knoester), 2020[51]	Multiscale modelling – MD (Herringbone arrangement), microelectrostatics and Frenkel exciton Hamiltonian, optimized with absorption spectra	Energetic and structural disorder, higher packing density in IW explained the spectral splitting
Patmanidis et al. (Marrink), 2020[46]	MD simulations (with brick layer, staircase and herringbone arrangements); Small-angle X-ray scattering	Brick layer and herringbone arrangements were plausible, brick layer being more stable. Interdigitated alkyl chains led to reduced widths between the two walls
Krishnaswamy et al. (Pshenichnikov), 2022[67]	Microfluidic flash dilution and Cryo-EM micrographs, compared to MD model	Inner wall remains unchanged and homogeneous during flash dilution
Patmanidis et al. (Marrink), 2022[68]	MD simulations on a coarse-grained model based on QM calculations and crystal structures of similar dyes	Time-dependent orientations of molecules during the assembly, model favors brick-layer arrangement

[a]C8O3 = 5,5',6,6'-tetrachloro-1,1'-dioctyl-3,3'-di-(3-carboxypropyl)-benzimidacarbocyanine

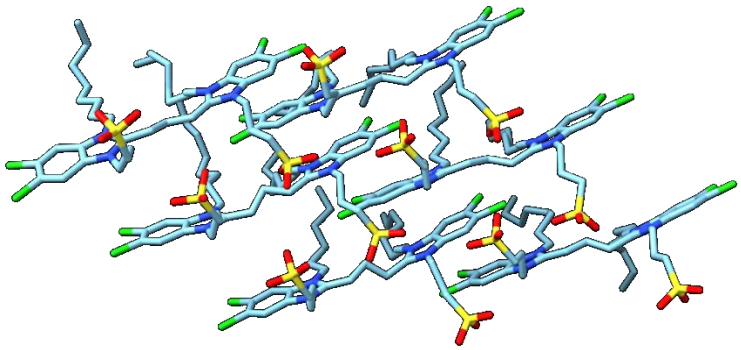

Extended Data Figure 1. Inner wall asymmetric unit (Hydrogen atoms are omitted for clarity).

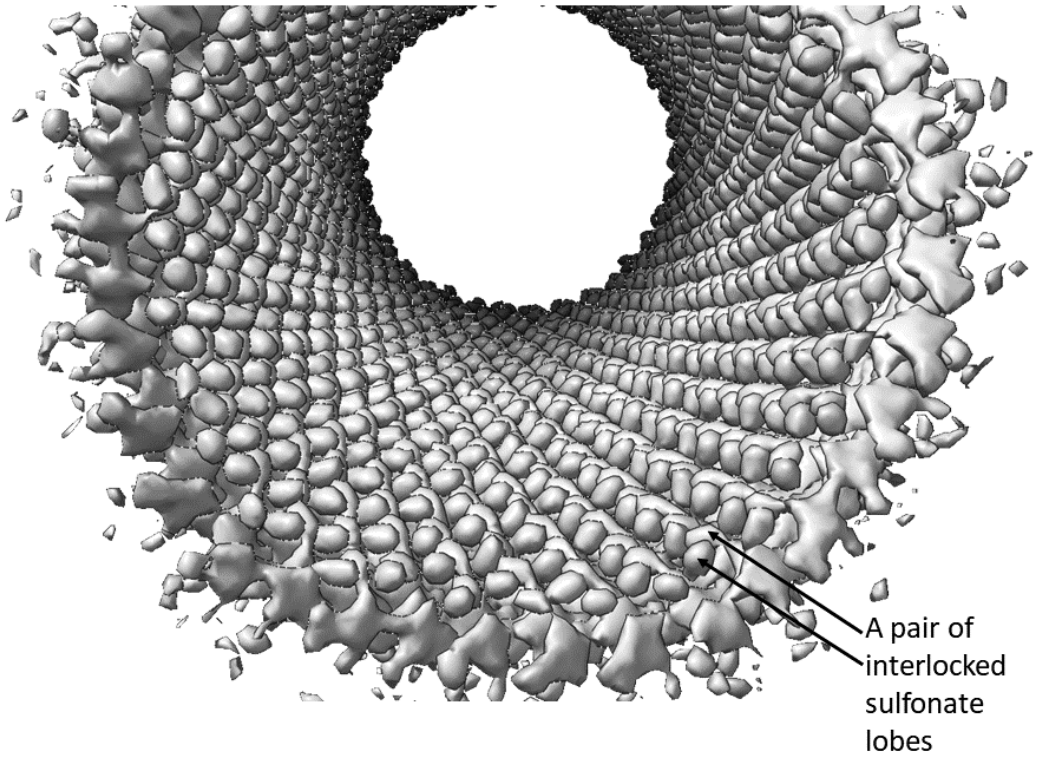

Extended Data Figure 2. A zoomed in inner wall density with cut away top-down view. The sulfonate lobes show a regular interlocked pattern.

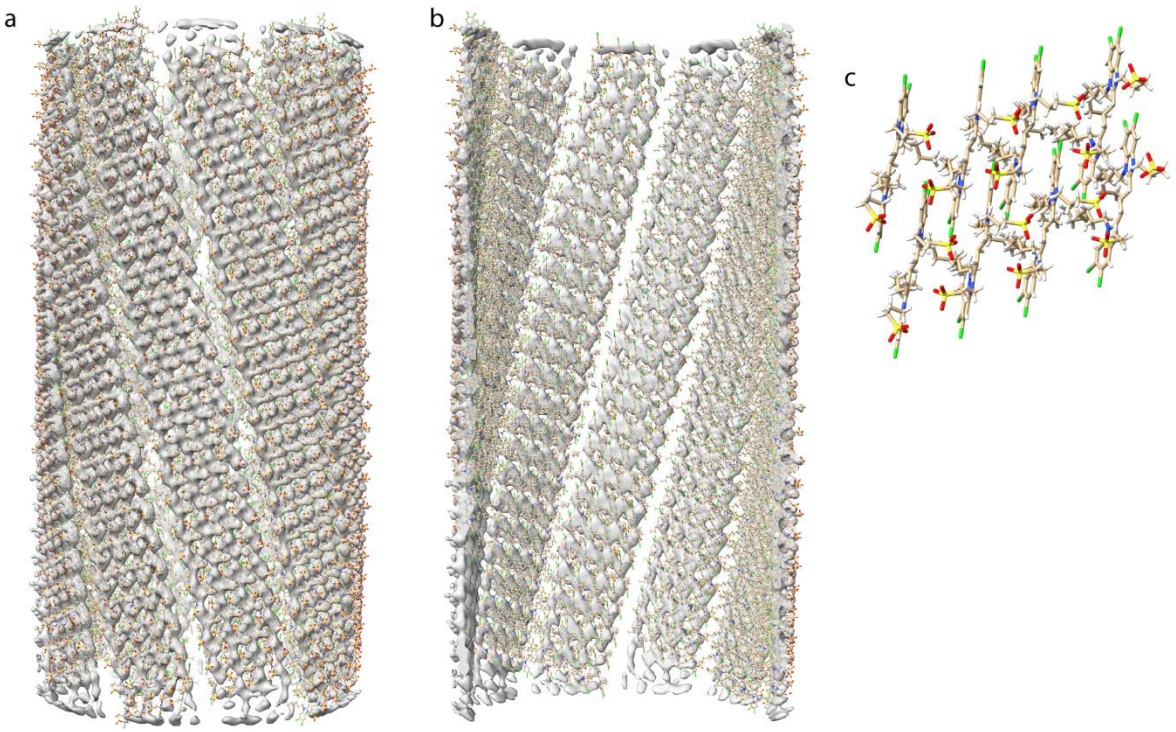

Extended Data Figure 3. Outer wall density overlayed with the fitted molecular model, a. side view, b. cut-away view, and c. asymmetric unit (ASU). The sulfonate interlocking can be seen in the outer wall as well.

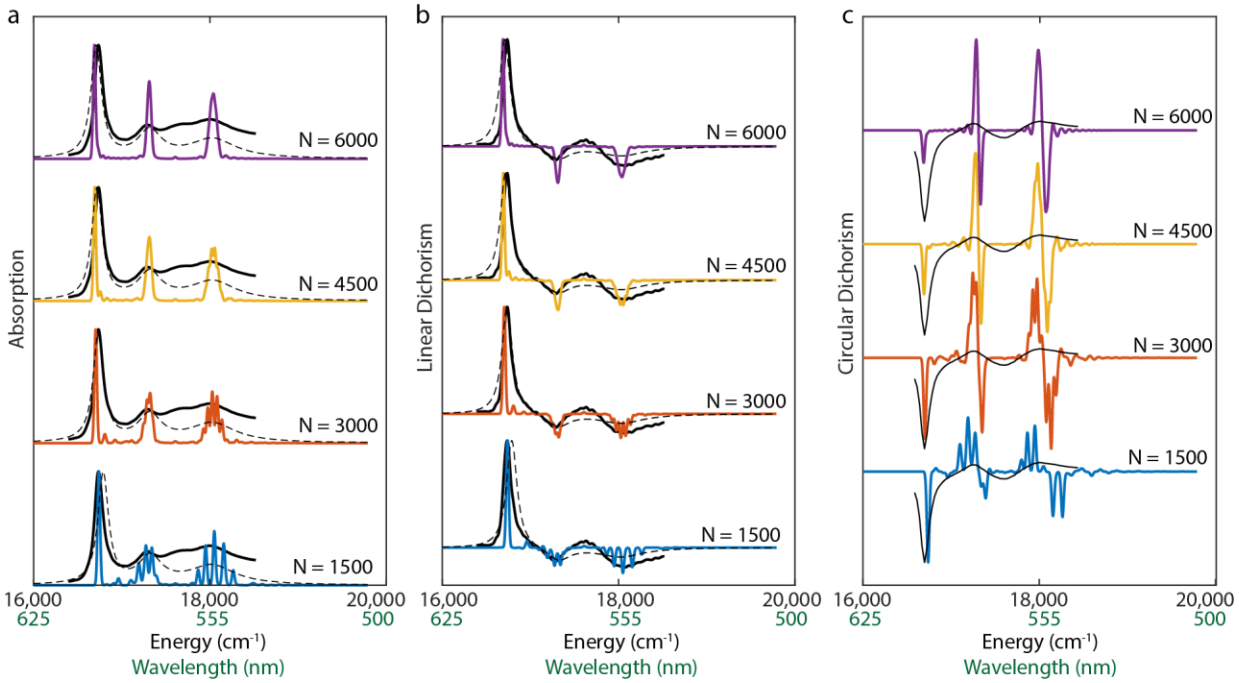

Extended Data Figure 4. a. Absorption, b. linear dichroism, and c. circular dichroism spectra of isolated inner walls of the LHNs. Solid black lines: experimental spectra; colored lines: spectra calculated from the dimerized Frenkel exciton Hamiltonian corresponding to inner wall structures of varying sizes, blue: 1500, red: 3000, yellow: 4500, and purple: 6000 monomers; dashed black lines: calculated spectra assuming periodic boundary conditions with added Lorentizian broadenings.

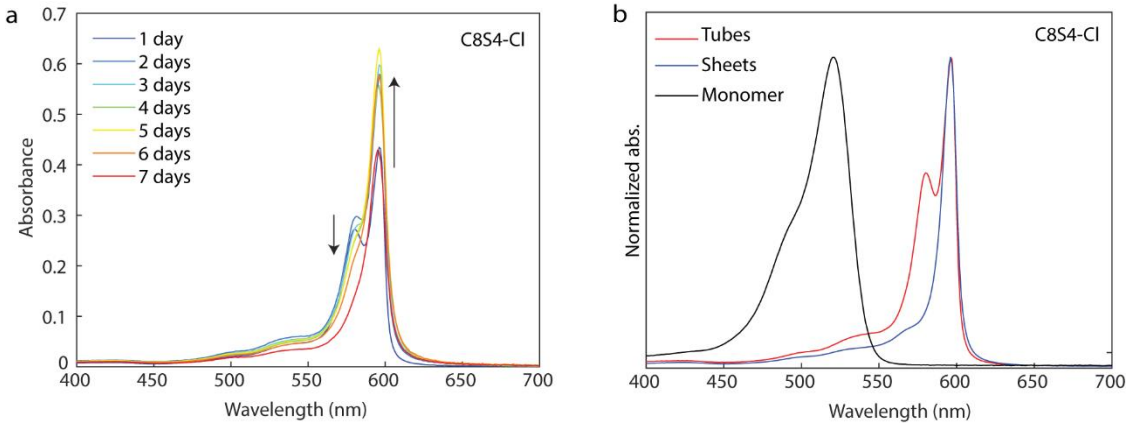

Extended Data Figure 5. a. Absorption spectra of C8S4-Cl aggregate made at 0.1 mM dye concentration and 5% MeOH over a course of 7 days showing conversion to sheet-like morphology, and b. normalized absorption spectra of the monomer in 100% MeOH (black), sheets in 20% MeOH (blue) and tubes in 5% MeOH (red) with 0.1 mm final dye concentration.